Novel Sol–Gel Synthesis of Acidic MgF$_{2-x}$(OH)$_x$ Materials

Stefan Wuttke,[a] Simona M. Coman,[a, b] Gudrun Scholz,[a] Holm Kirmse,[c] Alexandré Vimont,[d] Maro Daturi,[d] Sven L. M. Schroeder,[e, f] and Erhard Kemnitz*[a]

Abstract: Novel magnesium fluorides have been prepared by a new fluorolytic sol–gel synthesis for fluoride materials based on aqueous HF. By changing the amount of water at constant stoichiometric amount of HF, it is possible to tune the surface acidity of the resulting partly hydroxylated magnesium fluorides. These materials possess medium-strength Lewis acid sites and, by increasing the amount of water, Brønsted acid sites as well. Magnesium hydroxyl groups normally have a basic nature and only with this new synthetic route is it possible to create Brønsted acidic magnesium hydroxyl groups. XRD, MAS NMR, TEM, thermal analysis, and elemental analysis have been applied to study the structure, composition, and thermal behaviour of the bulk materials. XPS measurements, FTIR with probe molecules, and the determination of N$_2$/Ar adsorption–desorption isotherms have been carried out to investigate the surface properties. Furthermore, activity data have indicated that the tuning of the acidic properties makes these materials versatile catalysts for different classes of reactions, such as the synthesis of (all-rac)-[α]-tocopherol through the condensation of 2,3,6-trimethylhydroquinone (TMHQ) with isophytol (IP).

Keywords: heterogeneous catalysis · Lewis acids · magnesium fluoride · sol–gel processes · vitamins

Introduction

Several syntheses have been developed and are in use for inorganic metal fluorides, but sol–gel synthesis has recently become a powerful route for obtaining these materials.[1] The principle is based on the reaction of a metal alkoxide with anhydrous HF in alcoholic solution, resulting in an exchange of -OR by -F (fluorolysis); this forms a metal fluoride sol, which, under appropriate conditions, can be converted into the corresponding nanoscopic, pure Lewis acid metal fluoride.[2]

This method has been successfully employed for the synthesis of magnesium fluoride.[3,4] The resulting material is a pure Lewis acid and exhibits a remarkably high Lewis acidity in comparison with classically prepared magnesium fluorides.[3] This Lewis acid is able to catalyse the dismutation of CHClF$_2$ at 350 °C, which indicates a medium strength of the Lewis acidic sites.[5]

Magnesium oxide/hydroxide fluoride can be prepared by combining this synthesis with the synthesis of metal oxides.[6] The process consists of a two-step synthesis: 1) reaction of magnesium alkoxides with a substoichiometric amount (n < 2) of non-aqueous HF solution; 2) addition of a moderate excess of water (with respect to the remaining alkoxide groups) followed by calcination at 350 °C under Ar for 3 h. The resulting magnesium oxide/hydroxide fluoride has

[a] Dipl.-Chem. S. Wuttke, Prof. Dr. S. M. Coman, Priv.-Doz. Dr. G. Scholz, Prof. Dr. E. Kemnitz
Humboldt University Berlin, Institute of Chemistry
Brook-Taylor-Straße 2, 12489 Berlin (Germany)
Fax: (+49) 30-20937277
E-mail: erhard.kemnitz@chemie.hu-berlin.de

[b] Prof. Dr. S. M. Coman
University of Bucharest, Faculty of Chemistry
Department of Chemical Technology and Catalysis
Bdul Regina Elisabeta 4-12, 030016 Bucharest (Romania)

[c] Dr. H. Kirmse
Humboldt University Berlin, Institute of Physics
Newton-Str. 14, 12489 Berlin (Germany)

[d] Dr. A. Vimont, Prof. Dr. M. Daturi
Laboratoire Catalyse et Spectrochimie, UMR 6506
CNRS-ENSICAEN-Université de Caen
Boulevard du Maréchal Juin, 14050 Caen Cedex (France)

[e] Dr. S. L. M. Schroeder
School of Chemical Engineering and Analytical Science
The University of Manchester
Sackville Street, Manchester, M60 1QD (UK)

[f] Dr. S. L. M. Schroeder
School of Chemistry, The University of Manchester
Manchester, M13 9PL (UK)

Lewis and Brønsted base sites due to the O^{2-} and OH groups. Additionally, Lewis acid sites in the form of incompletely coordinated Mg^{2+} sites on the surface are also present. Such materials have been successfully applied as bifunctional catalysts in Michael addition reactions.[6]

In this paper, we report the structure and properties of nanoscopic, partly hydroxylated magnesium fluorides prepared by a novel sol–gel synthetic route. In a single step, aqueous HF solution was added to $Mg(OCH_3)_2$. By varying the concentration of the aqueous HF solution but keeping the molar ratio of HF to Mg constant at 2:1, different acidic materials were obtained. The bulk structure of these materials was investigated by XRD, TEM, and solid-state NMR. The thermal behaviour of the compounds was investigated by DTA/TG coupled with MS measurements. The surface properties were examined by means of N_2 and Ar adsorption–desorption isotherms, XPS, and infrared investigations with probe molecules. Furthermore, catalytic test reactions have been carried out to investigate the different acid sites.

To our astonishment, the resulting magnesium hydroxyl groups on magnesium fluoride are purely acidic, and to the best of our knowledge this is the first time that this has been reported on. Magnesium hydroxide groups on magnesium fluoride and general magnesium hydroxide have been discussed in the literature as basic species[7,8] and have been applied as basic catalysts.[9–11] In contrast, our new materials have proved to be very active in reactions requiring acidic sites. Thus, we have successfully applied these compounds as heterogeneous catalysts for the synthesis of (all-*rac*)-[α]-tocopherol.

Experimental Section

Sample preparation

Synthesis of $MgF_{2-x}(OH)_x$ samples: Five magnesium fluoride catalysts were prepared from metallic Mg using the sol–gel method, as follows: metallic Mg (Aldrich, 99.98 % powder) (1.56 g, 64 mmol) was treated with dry methanol (50 mL) at room temperature overnight. After heating under reflux conditions for 3 h, a stoichiometric amount of HF (130 mmol) dissolved in different amounts of water (HF solution concentrations: 40, 57, 71, 87, and 100 wt % HF) was added to the formed Mg-$(OCH_3)_2$ solution. The mixtures reacted to form highly viscous transparent gels. After ageing for 12 h, each gel was dried under vacuum at room temperature. The solid product thus obtained was then further dried under vacuum at 70 °C for 5 h. The prepared catalysts are referred to hereafter as MgF$_2$-40, MgF$_2$-57, MgF$_2$-71, MgF$_2$-87, and MgF$_2$-100, indicating the different concentrations of HF solutions used. For comparison, crystalline commercial MgF$_2$ (Aldrich, 99.8 %) was also tested (MgF$_2$-C).

Synthesis of (all-*rac*)-[α]-tocopherol: In a typical procedure, 2,3,5-trimethylhydroquinone (TMHQ, 152 mg, 1 mmol) was dissolved in a 1:1 mixture of heptane/propylene carbonate (6 mL) in a glass vial with a standard capacity of 8 mL, equipped with a magnetic stirrer. Isophytol (IP, 296 mg, 1 mmol) and catalyst (50 mg) were then added. After sealing the vial, it was immersed in an oil bath at 100 °C, and the reaction mixture was stirred at 1500 rpm for 60–1200 min. After separating the catalyst from the two-phase solvent mixture, the heptane phase containing the tocopherol was isolated and the solvent was removed in vacuo to give the crude product. The crude products were analysed by HPLC (column: EC 125/4.6 Nucleosil 120-5 C18; eluent: acetonitrile; flow rate: 0.8 mL min^{-1}; wavelength: 280 nm; volume of sample: 15 μL) and by ^1H and ^{13}C NMR

(Bruker AV 400 spectrometer; samples in CDCl$_3$ solution with Me$_4$Si as internal standard). 2,3,5-Trimethylhydroquinone (97 wt. %) and isophytol (95 wt. %) were purchased from Acros Organics. The other reagents (analytical grade) were obtained from Merck.

Characterisation

XRD: X-ray powder diffraction (XRD) patterns were recorded using an XRD-7 Seiffert-FPM diffractometer equipped with a Cu$_{K\alpha}$ radiation source.

^{19}F MAS NMR: Solid-state MAS NMR experiments were performed on a Bruker AVANCE 400 spectrometer by using a 2.5 mm rotor for ^{19}F ($\nu_{Larmor}(^{19}F) = 376.4$ MHz) with the appropriate Bruker MAS probe head and applying different spinning frequencies. The spectrometer was calibrated with standard reference substances (^{19}F: C$_6$F$_6$ as secondary standard $\delta_{iso} = -166.61$ ppm against CFCl$_3$). Background ^{19}F signals could be suppressed by application of a phase-cycled depth pulse sequence according to Cory and Ritchey.[12]

Elemental analysis: The C, H, N contents were determined using a Leco CHNS-932 analyser. The fluoride content was determined by means of a fluoride-sensitive electrode. Before the analysis, the samples were digested by fusion with Na$_2$CO$_3$/K$_2$CO$_3$. The magnesium contents of the samples were determined by the ICP OES method (IRIS Intrepid HR DUO) after a microwave-assisted (ETHOS plus) digestion with HNO$_3$.

Determination of the surface area and porosity: The surface properties of the samples were determined by acquiring adsorption–desorption isotherms of N_2 at 77 K and of Ar at 87 K on a Micromeritics ASAP 2020 instrument. Samples were first degassed in vacuo at 70 °C. Surface areas were calculated according to the BET method.[13]

Thermal analysis: Thermal analysis experiments were performed on a Netzsch STA 409 C apparatus. A DTA-TG sample-holder system (Pt/PtRh10 thermocouple) was used, and measurements were performed in an atmosphere of N_2. The thermo analyser was equipped with a Balzers QMG 429 quadrupole mass spectrometer for the multiple ion detection modes.

Transmission electron microscopy (TEM): MgF$_2$-71 nanoparticles for TEM measurements were prepared by dispersing the powder in methanol and applying ultrasound. A conventional carbon film of thickness about 20 nm supported by a copper grid was then dipped into the suspension. The grid was slowly moved sideways to pick up as many particles as possible. After complete evaporation of the methanol from the specimen, the particles were studied on a JEOL TEM 2200FS operated at an acceleration voltage of 200 kV. In high-resolution mode TEM (HRTEM), the point-to-point resolution was 0.19 nm and the information limit for the visualisation of crystal lattice planes was 0.14 nm.

FTIR spectroscopy: Samples were pressed (10^7 Pa) into self-supported discs (2 cm^2 area, 10–20 mg cm^{-2}). All samples were then degassed in situ before measurement at 373 K. The infrared cell was made of quartz and was equipped with CaF$_2$ windows. A movable quartz sample holder allowed the pellet to be moved into the infrared beam for spectral acquisition or into a furnace at the top of the cell for thermal treatment. Transmission IR spectra were recorded in the range 650–4000 cm^{-1} on a Nicolet Nexus spectrometer equipped with an extended KBr beam-splitting device and a mercury cadmium telluride (MCT) cryodetector. The cell was connected to a vacuum line for evacuation, calcination steps ($P_{residual} = 10^{-3}$–10^{-4} Pa), and for the introduction of CO gas into the infrared cell. Spectra were recorded at room temperature. In the CO adsorption experiments, the temperature of the pellet was decreased to about 100 K by cooling the sample holder with liquid N_2 after quenching the sample from the thermal treatment temperature. CO (> 99.997 % pure, supplied by Air Liquide, France) was provided from a gas balloon, dried with liquid N_2, and incrementally dosed to the sample.

The addition of accurately known increments of CO probe molecules to the cell (a typical increment corresponded to 100 μmol of CO per gram of material) was possible by means of a calibrated volume (2.15 cm^3) connected to a pressure gauge for the control of the probe pressure (1–10^4 Pa range). The CO pressure inside the IR cell was controlled by another pressure gauge (1–10^3 Pa range).

X-ray photoelectron spectroscopy (XPS): High-resolution X-ray photo-electron spectroscopy (XPS) was performed with a Kratos Axis Ultra electron spectrometer with a monochromated $Al_{K\alpha}$ source ($h\nu =$ 1486.6 eV) operating at 180 W and the analyser operating in CAE20 mode. Before recording the spectra, the samples were degassed overnight in a load lock chamber at a pressure $< 10^{-6}$ mbar. The vacuum in the spectrometer chamber was $< 10^{-8}$ mbar. The binding energy scale was referenced to the aliphatic C 1s peak at 284.8 eV. The charge neutralisation system of the Kratos system was used during data acquisition. The spectrometer energy scale was calibrated according to ISO 15427.[14] Fitting analysis of the data was performed with the XPSPeak 4.1 package, using Gaussian/Lorentzian lines with 20% Gauss character. For the analysis of the Mg 2p data, a spin-orbit splitting of 0.28 eV was assumed.[15, 16]

Results and Discussion

Preparation of the catalysts

The non-aqueous sol–gel route for obtaining pure Lewis acidic metal fluorides has been described above. In addition to the described fluorolysis with pure HF, the reaction was also performed in the presence of different amounts of water, thereby facilitating partial hydrolysis of the M−OR bond resulting in an M−OH bond.[17,18] By adjusting the molar ratio of the metal alkoxides, the stoichiometry of $M(OR)_x$ to HF remains constant at 1:x, but by varying the water content at the same time, the hydrolysis should become increasingly competitive with increasing amount of water. As a consequence, in addition to fluorolysis, this results in increasingly hydroxylated metal fluorides.[19]

We successfully applied this general approach for a *one-pot* sol–gel synthesis of different partially hydroxylated magnesium fluoride phases (Scheme 1).

$$Mg(OCH_3)_2 \; + \; 2\,HF \; + \; (x+y)\,H_2O$$

$$\downarrow$$

$$MgF_{2-x}(OH)_x \; + \; 2\,CH_3OH \; + \; x\,HF \; + \; y\,H_2O$$
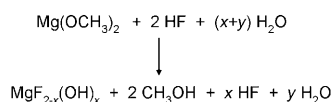
Scheme 1. Schematic representation of the one-pot sol–gel synthesis of different $MgF_{2-x}(OH)_x$ phases.

The general approach of the synthesis involves the reaction of magnesium methoxide with HF (molar ratio 1:2) dissolved in varying amounts of water (as described above in the Experimental Section). In contrast to the non-aqueous sol–gel route, which results in the formation of clear sols and transparent gels, the aqueous route results in opaque gels.[4] The resulting gels were dried in vacuo at 70 °C for 5 h to yield the xerogels. The bulk and surface structures and the thermal behaviour of these materials were then investigated.

Catalyst characterisation

Investigation of the bulk properties
XRD measurements: All of the respective $MgF_{2-x}(OH)_x$ samples exhibited only three broad reflections in their X-ray powder diffractograms (as shown in Figure 1a). X-ray interference stems from spectral and geometrical broadening effects (which are the same for Figures 1a and b) and crystalline size. From the observed patterns, it was clear that our samples consisted of very small crystallites, giving rise to three broad reflections at the typical positions of MgF_2 (Figure 1b).
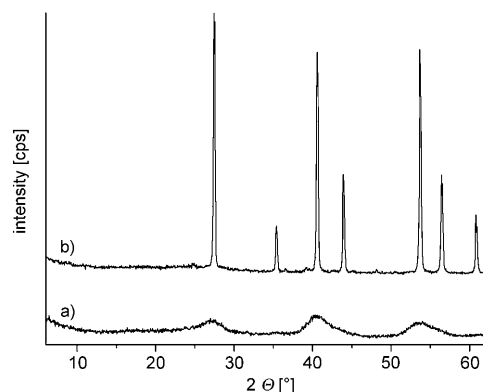

Figure 1. a) Typical X-ray powder reflections of MgF_2 samples prepared by the sol–gel route; b) X-ray pattern of crystalline MgF_2 (MgF_2-C).

TEM measurements: Figure 2 shows an HRTEM image of the MgF_2-71 sample, in which the morphology and size of the crystalline particles are indicated by an individual set of
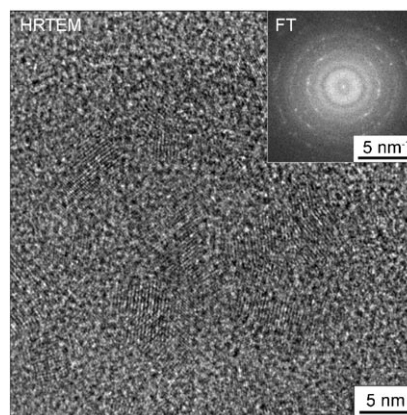

Figure 2. HRTEM image of an MgF_2-71 cluster on a carbon support film. The inset shows the Fourier transform of the HRTEM image, in which the radial distance represents the lattice fringe distance.

lattice planes. The particles exhibit different types of morphology. Some particles appear almost circular in the projection, hinting at a spherical shape. Other particles are bounded by straight lines, indicating the formation of facets. The lateral size of the particles ranges from 30 to about 80 Å, resulting in a mean size of 50 Å.

In order to determine the structure of the crystalline phase, the interplanar distances between the various sets of lattice planes were measured by means of digital image

analysis. The inset in Figure 2 shows a Fourier transform (FT) of the HRTEM image. The radial distance of the apparent spots indicates the lattice distance in reciprocal space. A comparison with tabulated values for MgF$_2$ shows very good agreement. The lateral position of the spots corresponds to the orientation of the lattice fringes. Since the spots are statistically distributed around the circles, a textured alignment of the nanocrystals can be ruled out.

The carbon support film is visible in the surrounding of the cluster (see the upper-left area in Figure 2). It shows the typical HRTEM contrast of an amorphous material. The same contrast is seen between the MgF$_2$-71 nanocrystals. By X-ray diffraction analysis, crystalline areas of MgF$_2$ beside the amorphous areas can be identified.

^{19}F MAS NMR spectroscopy: The fluorine coordination in the respective MgF$_2$ samples was investigated by high-resolution ^{19}F MAS NMR (spectra shown in Figure 3). Magnesi-
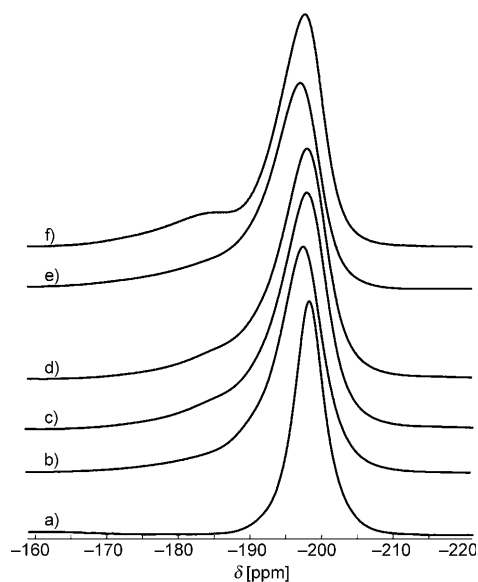

Figure 3. ^{19}F MAS NMR spectra of a) MgF$_2$-C, b) MgF$_2$-100, c) MgF$_2$-87, d) MgF$_2$-71, e) MgF$_2$-57, and f) MgF$_2$-40.

um fluoride crystallises in the rutile-type structure, in which each Mg^{2+} ion is surrounded by six crystallographically equivalent F$^-$ ions, and each F$^-$ ion is coordinated to three Mg^{2+} ions.[20] Accordingly, the spectrum of MgF$_2$-C shows only one sharp symmetrical signal at $\delta = -198$ ppm, which can clearly be assigned to MgF$_6$ species in crystalline MgF$_2$.[4,6] The dominant fluorine signal of all of the present samples is at almost the same position as that of crystalline MgF$_2$, indicating that the coordination of the dominating fluorine species remains nearly the same. Upon decreasing the HF concentration from 100 wt% to 40 wt%, there is an increase in a small asymmetrical shoulder in the low-field part of the spectrum. A similar shoulder has been observed in the ^{19}F MAS NMR spectrum of magnesium oxide/hydroxy-

fluoride.[6] We thus surmise that the local coordination of Mg may change from MgF$_6$ to MgF$_5$O or MgF$_4$O$_2$ units.[6]

^{19}F MAS NMR studies on crystalline AlF$_x$(OH)$_{3-x}$·H$_2$O samples also showed a low-field shift in the fluorine signal with increasing amount of hydroxyl groups.[21] Therefore, with decreasing HF concentration, and hence increasing H$_2$O concentration, the amount of hydroxyl groups in the final MgF$_2$ increases, and this is reflected in the appearance of the low-field shift in the ^{19}F spectra.

Elemental analysis: Table 1 summarises the mass percentages of Mg, F, C, and H in the synthesised samples. The theoretical values for Mg and F in MgF$_2$ are 39 and 61%, respectively. Although molar ratios of HF to magnesium were used in the sol–gel synthesis, the fluorine contents in the obtained materials were lower than that in pure MgF$_2$. Nevertheless, the F:Mg molar ratio in the products was close to 2 in all cases, showing that the main composition of the prepared samples was MgF$_2$, which was also indicated by other techniques. Apart from MgF$_2$-100, the samples were free from carbon, which indicates a complete solvolysis process.

Table 1. Mass percentages of Mg, F, C, and H as determined by elemental analysis of the studied compounds.

HF [wt%]	100	87	71	57	40
F	50.4	48.5	50.7	50.1	49.3
C	3.3	0	0	0	0
H	1.5	1.5	1.2	1.6	1.4
Mg	33.3	33.2	31.1	32.3	30.4
Σ	88.5	83.2	83	84	81.1
overall sum[a]	100.1[b]	99.8	99.5	99.4	99.1
F/Mg molar ratio	1.9	1.9	2.1	2	2.1

[a] Mass of water determined by DTA-TG measurements. [b] With consideration of the loss of the methoxy groups.

A common feature of all of the samples was that the sum of the Mg and F mass percentages did not amount to 100% (see Table 1). As evidenced by DTA-TG-MS (next paragraph), this mass difference was perfectly consistent with the liberation of water above 100°C. Thus, for example, the sum of weight percentages for sample MgF$_2$-71 amounted to 81.7% (without hydrogen) and the water loss determined by TA was exactly 17.8%, the overall sum being 99.5%. Since the molar ratio of F to Mg was near to 2 and in agreement with the results from NMR and TEM, there could not be a large amount of hydroxyl groups in this sample. The same situation was found for all of the other samples. Consequently, the difference between the sum of the masses shown in Table 1 and 100% can, to a good approximation, be mainly ascribed to water adsorbed at the surface acid sites of the samples.

Thermal behaviour: The major weight loss of all but one of the samples is due to the loss of water, which is accompanied by a broad endothermic signal between 110 and 220°C in the DTA curves (as shown for MgF$_2$-71 in Figure 4). The only exception is the MgF$_2$-100 sample, which shows a significant loss of methoxy groups, confirming the elemental anal-
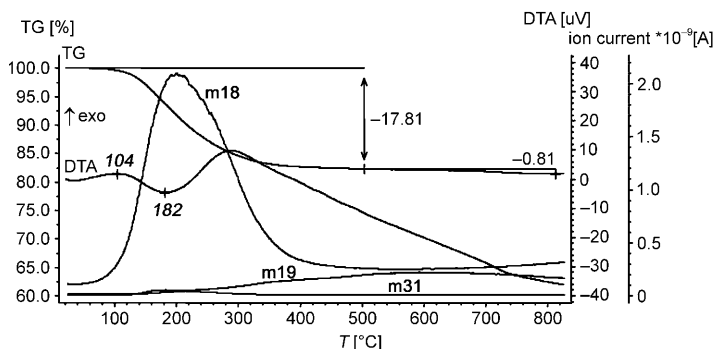
Figure 4. TA/MS curves of MgF$_2$-71 with the IC curves for m/z 18 (H$_2$O$^+$), m/z 19 (F$^-$), and m/z 31 (CH$_3$O$^+$).

ysis results. The DTA curves also feature one broad exothermic signal between 220 and 380 °C.

The X-ray patterns of the phases that remained after heating to 800 °C showed in each case the reflections of crystalline MgF$_2$. Hence, the broad peak in the DTA curves was clearly due to the onset of crystallisation, which is in agreement with previous studies on non-aqueous sol–gel prepared MgF$_2$.[4]

Investigation of the surface properties

IR spectra after activation: Spectra of the respective MgF$_2$ samples activated at 100 °C in vacuum were similar in shape. All spectra featured a broad and complex ν(OH) band between 3600 and 2800 cm^{-1} due to residual adsorbed water and/or hydroxyl groups in the bulk and/or on the surface. The presence of water was confirmed by a band at 1650 cm^{-1}.

Adsorption of CO: CO is one of the best probe molecules to characterise Lewis acidic surfaces since it is only moderately basic, and is therefore more selective than other frequently used probe molecules such as NH$_3$ and pyridine.[22] It interacts by the free electron pair of the carbon atom bonding to an acid site on the surface, resulting in a blue shift of the CO stretching vibration band. The higher the blue shift is, the higher the strength of the Lewis acidity. If the density of d states is too low, or does not exist, as in MgF$_2$, back donation of electron density from the metal to the CO orbital is negligible. Furthermore, CO allows the discrimination of Lewis acid sites and enables the detection of Brønsted acid sites of various strengths and with different accessibilities.

Difference IR spectra of the CO stretching region of adsorbed CO on the respective magnesium fluoride samples are shown in Figure 5. The spectra of the MgF$_2$-100 and MgF$_2$-87 samples are similar in shape, with a band at 2200–2165 cm^{-1} having a maximum at 2180 cm^{-1} and a small shoulder at 2165–2150 cm^{-1}. The spectra of the other three samples (MgF$_2$-71, MgF$_2$-57, and MgF$_2$-40) show the same band at 2200–2165 cm^{-1} with a maximum at 2184 cm^{-1}, but additionally feature a band at 2165–2150 cm^{-1} with a maximum at 2160 cm^{-1}.

The observed ν(CO) stretching vibrations at 2180–2200 cm^{-1} can be assigned to Lewis acidic centres of medium strength.[23] It is more difficult to assign the band at 2165–2150 cm^{-1} because of overlap of the vibrational bands assigned to CO coordinated to weak Lewis and Brønsted acidic centres in this region. It was found that the observed
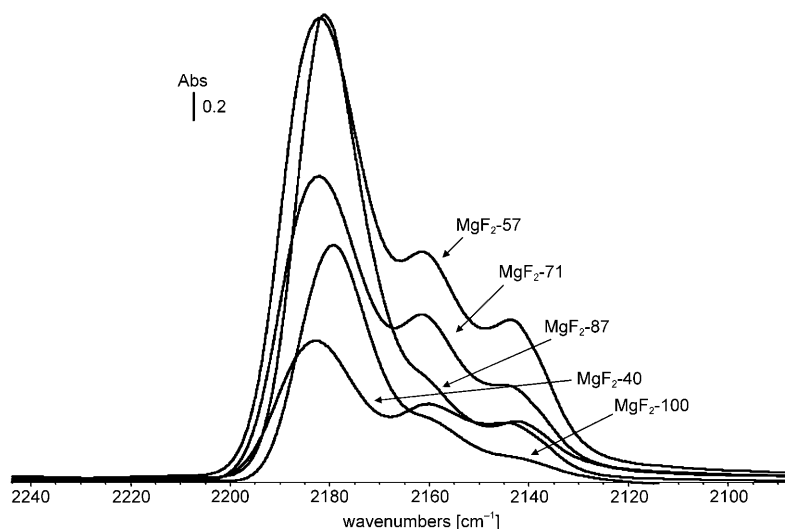

Figure 5. IR difference spectra of each of the respective magnesium fluorides recorded at 100 K after the adsorption of CO at equilibrium pressure (mass-normalised).

blue shift in the CO vibration in this region can be attributed to its coordination to fivefold coordinated Mg^{2+} ions on the surface.[24] Therefore, it is hard to distinguish between coordinative CO interactions and H-bonding interactions with hydroxyls, a problem that is exacerbated by the fact that the hydroxyl region is mainly hidden by the presence of a broad absorption related to the presence of water. Consequently, a more specific probe molecule is required to differentiate between the two types of acidic sites.

Adsorption of lutidine: Lutidine (2,6-dimethylpyridine) is a probe molecule that is particularly well-suited for the detection of Brønsted centres on solids. As a result of its stronger basicity and lower affinity for Lewis acid sites in comparison to pyridine (due to the steric hindrance of its methyl groups), it is a more suitable candidate for probing Brønsted acid sites.[25]

The IR spectra of adsorbed lutidine on MgF$_2$-71, MgF$_2$-57, and MgF$_2$-40 are similar in shape and show three bands at 1575–1590 cm^{-1}, representing the ν_{8a} mode of the liquid

phase; 1610–1620 cm^{-1}, attributable to the ν_{8b} mode of molecules weakly coordinated to Lewis acid sites; and 1625–1635 and 1635–1660 cm^{-1}, characteristic of protonated species. Figure 6 shows the IR difference spectra of MgF$_2$-71, as a representative of these three samples, after adsorption of lutidine followed by evacuation at 273, 323, and 373 K. On increasing the temperature, the physisorbed and weakly coordinated species are lost, while the protonated species persist. According to the data reported by Oliviero et al.,[25] the band at wavenumber 1653 cm^{-1} represents a lutidinium species and is indicative of medium-strength Brønsted acidic sites. The amount of this species increases according to MgF$_2$-40 < MgF$_2$-71 ≤ MgF$_2$-57.
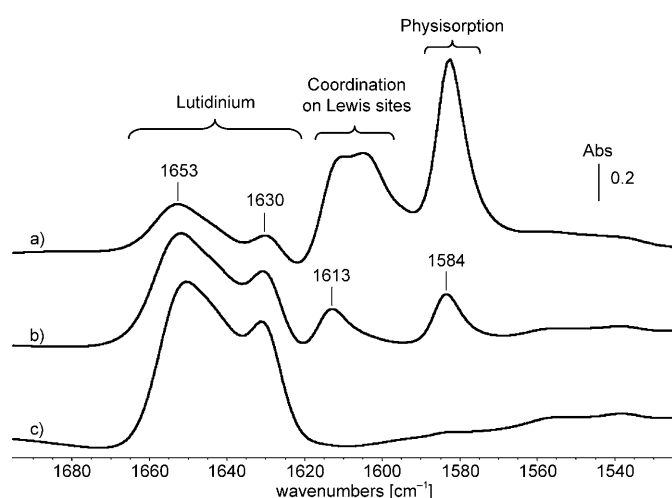

Figure 6. IR difference spectra recorded after introduction of lutidine on MgF$_2$-71, 1 Torr at equilibrium pressure, followed by desorption in vacuo for 15 min at a) 273 K, b) 323 K, and c) 373 K.

The IR spectra of lutidine adsorbed on MgF$_2$-87 and MgF$_2$-100 were found to be different. The main bands in these spectra could be assigned to physisorbed and weakly coordinated lutidine, while no protonated lutidine species were detected.

Comparing these results with those obtained for CO adsorption, we conclude that MgF$_2$-87 and MgF$_2$-100 have only Lewis acid sites. Therefore, the small shoulder at 2165–2150 cm^{-1} observed after CO adsorption corresponds to absorption at weak Lewis sites that are probably due to five-fold coordinated Mg^{2+}. In the case of MgF$_2$-71, MgF$_2$-57, and MgF$_2$-40, the band at 2165–2150 cm^{-1}, which has a different shape and intensity, is believed to represent both weak Lewis acidic sites and medium-strength Brønsted acidic sites.

Adsorption of CO$_2$: Carbon dioxide is acidic and it is adsorbed specifically at basic hydroxyl groups forming hydrogencarbonate species or at basic oxygen ions forming different kinds of carbonate species.[26] Due to hydrolysis of Mg−OCH$_3$ bonds resulting in Mg−OH bonds, basic OH groups are to be expected, as in Mg(OH)$_2$, for which CO$_2$ is a sensi-

tive probe molecule. Additionally, CO$_2$ interacts with undercoordinated cations (Lewis acid sites) on the surface, whereupon the molecule loses its centre of symmetry but still retains its linear shape ($D_{8h} \rightarrow C_{8v}$). Spectroscopically, the consequences of this interaction are the appearance of a strong band (or bands) in the 2400–2300 cm^{-1} range and a weak band (or bands) in the 1400–1370 cm^{-1} range.[27]

All samples show the same spectrum after the adsorption of CO$_2$, as exemplified for the case of MgF$_2$-71 in Figure 7. A strong band near 2355 cm^{-1} and a weak band at 1385 cm^{-1} appeared after CO$_2$ adsorption. In accordance with the findings of different authors,[28,29] these bands can be attributed to linearly adsorbed CO$_2$ molecules at Lewis acid centres, which must be undercoordinated Mg^{2+} sites on the surface. Furthermore, it can be stated that there is no perturbation in the OH band region, indicating that neither hydrogencarbonate species nor carbonate species are present in any of the samples. Consequently, no basic hydroxyl groups or oxygen atoms are present on the surface of any of these samples, making them completely different to MgO.[30]
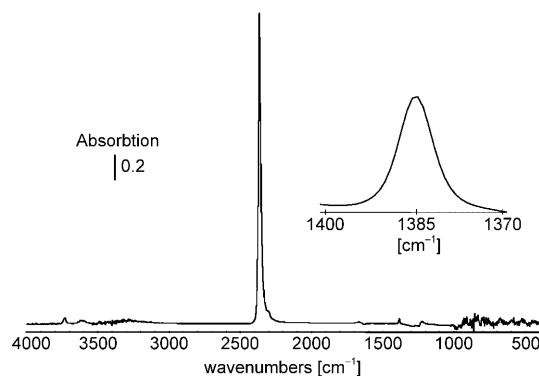

Figure 7. IR difference spectrum recorded after introduction of CO$_2$ on MgF$_2$-71, 1 Torr at equilibrium pressure. Inset: enlargement of the spectrum in the 1400–1370 cm^{-1} range.

XPS measurements: The elemental compositions and chemical states of the samples were characterised by XPS, probing the elements Mg, O, and F. For the anions, we not only examined the commonly used F 1s and O 1s emissions, but also the low-binding-energy (low-BE) O 2s and F 2s emissions. These low-BE emissions are more bulk-sensitive because of the higher kinetic energy of the photoelectrons, which results in an inelastic mean free path (IMFP) of approximately 43 Å as compared to 31 Å for the O 1s emission and 27 Å for the F 1s emission.[31] Assuming spherical particle shapes, the surface areas of the materials would suggest particle radii that decrease from about 65 Å for MgF$_2$-40, to 49 Å for MgF$_2$-57, and to 43 Å for MgF$_2$-71. These radii exceed the IMFPs and hence some qualitative discrimination between the near-surface and bulk structures should be possible for these materials. In contrast, within the spherical shape model, MgF$_2$-87 and MgF$_2$-100 appear to have particle diameters of around 28 Å, which are comparable to the

IMFPs and should therefore result in less surface-to-bulk discrimination through use of the different emission lines.

For all of the samples, the rather bulk-sensitive (electron IMFP: 42 Å) Mg 2p emission (Figure 8, Table 2) could be fitted with a single Gaussian/Lorentzian line centred at BE values between 51.4 eV and 51.7 eV. These BE values are very close to (or only very slightly higher than) the Mg 2p BE that we determined for crystalline MgF_2 powder (51.4 eV). This finding is in line with the ^{19}F MAS NMR and elemental analysis results, which suggested bulk compositions close to the ideal MgF_2 chemical composition. Nevertheless, the Mg 2p emission lines of the high-surface-area materials are invariably broadened (FWHMs: 2.0–2.3 eV; Table 2) relative to those of crystalline MgF_2 (FWHM: 1.76 eV; Table 2), suggesting that significant fractions of Mg

species in these materials are in a chemical environment that differs from that in crystalline MgF_2.

Most importantly, the highest Mg 2p BE shift and the most pronounced broadening were detected for MgF_2-71 (Table 2), which is the most chemically heterogeneous material, exhibiting not only the highest Brønsted activity (as probed by its performance in the synthesis of tocopherol) but also Lewis acidity. The slightly raised Mg 2p BE suggests the presence of electron-deficient Mg^{2+} species, and is in line with the presence of Lewis acid centres, as probed by FTIR measurements on CO adsorption.

Turning to the emission lines from fluorine, we first compare the relative F 1s/Mg 2p emission intensity ratios in Figure 9. For comparison, the intensity ratios determined for crystalline MgF_2 have been normalised to 1. It can be seen that the intensity ratios of the rather more bulk-sensitive F 2s emissions from all of the samples are, within the error range, identical to the observed ratio in crystalline MgF_2. In contrast, the more surface-sensitive F 1s emissions from several of the different MgF_2 samples (40, 71, 100) are consis-
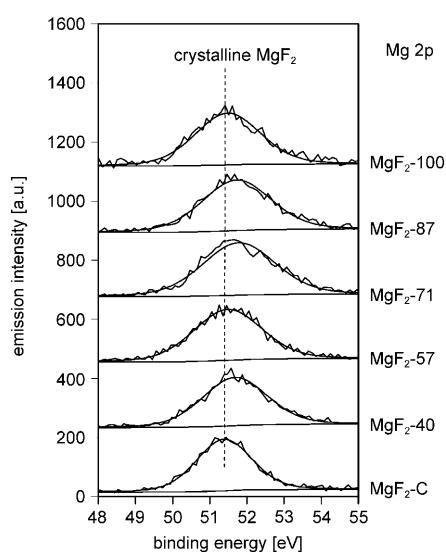

Figure 8. Mg 2p emissions from the various samples. All spectra have been scaled to approximately the same intensity at the maximum of the emission line.
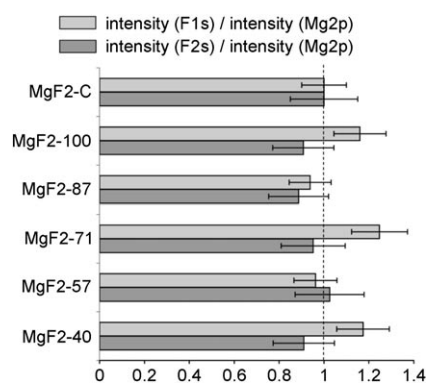

Figure 9. Bulk vs surface emission intensities for fluorine. Light-grey bars: ratios of the intensities of the emissions from F 1s and Mg 2p; dark-grey bars: ratios of the intensities of the emissions from F 2s and Mg 2p.

Table 2. Detailed XPS results of Mg, O, and F.

	Mg 2p			F 2s			F 1s			O 2s			O 1s		
	BE [eV]	I [%]	FWHM [eV]	BE [eV]	I [%]	FWHM [eV]	BE [eV]	I [%]	FWHM [eV]	BE [eV]	I [%]	FWHM [eV]	BE [eV]	I [%]	FWHM [eV]
MgF_2-40	51.6	100	2.00	31.1	100	2.90	686.1	93	2.24	27.1	100	1.93	534.8	38	1.70
							688.7	7	1.99				532.8	62	2.18
MgF_2-57	51.4	100	2.06	30.9	100	2.75	685.9	96	2.30	26.1	100	1.92	533.7	62	2.13
							688.0	4	1.58				532.0	38	1.72
MgF_2-71	51.7	100	2.28	31.1	100	2.73	685.9	82	2.27	27.7	100	4.64	534.4	53	2.68
							687.2	18	2.40				532.5	47	2.67
MgF_2-87	51.6	100	2.15	31.0	100	2.70	686.2	98	2.34	27.2	100	1.81	533.8	57	2.50
							688.5	2	1.37				532.3	43	2.18
MgF_2-100	51.4	100	2.05	30.8	100	2.59	685.9	92	2.07	27.6	100	3.28	532.9	100	2.99
							687.3	8	2.43						
MgF_2-C	51.4	100	1.76	30.8	100	2.35	686.0	100	1.96	–	<1	–	532.1	100	2.67
$Mg(OH)_2$	49.5	64	1.02	–	<1	–	–	<1	–	23.8	100	2.86	531.2	100	1.19
	50.3	36	1.69												
MgO	49.2	75	1.49	–	<1	–	–	<1	–	24.7	42	4.09	531.5	50	2.38
	50.2	25	2.02							21.1	58	2.57	529.6	50	1.55

tently higher than that from crystalline MgF$_2$. Samples MgF$_2$-87 and MgF$_2$-57 exhibit, within the error ranges, an F 1s/Mg 2p emission ratio that is slightly below or identical to that from MgF$_2$-C. A higher F 1s/Mg 2p emission ratio suggests that the surface regions of the sol–gel derived samples either incorporate an excess of F species or that the emission from the Mg centres is more efficiently shielded than in crystalline MgF$_2$, for example due to the presence of additional adsorbates such as H$_2$O or hydroxylic or hydroxidic species (see the discussion of O 1s features below).

The binding energies of the more bulk-sensitive F 2s emission materials range from 30.8 to 31.1 eV (Table 2), and so are very close to, or slightly higher than, the value of 30.8 eV obtained for crystalline MgF$_2$. This suggests that most fluorine species present in the samples are fluoridic and in an environment close to that in MgF$_2$. However, relative to crystalline MgF$_2$, the FWHM values for the F 2s emissions from all of the samples are elevated by approximately 0.3–0.4 eV, indicating that a range of F species with electronic structures different from the F-sites in crystalline MgF$_2$ are present. In fact, the slightly elevated BE values for some of the F 2s emissions could be indicative of fluorine species with reduced electron density, possibly due to competition for electron density from the Mg centres in the presence of additional hydroxylic or hydroxidic species, or due to the disturbances in the MgF$_2$ lattice of the non-crystalline samples. This would lead to the formation of F species with reduced Mg coordination, and hence reduced electron density, relative to the bulk F species in crystalline MgF$_2$.

These suggestions are supported by the more surface-sensitive F 1s emissions (Figure 10, Table 2), which also exhibit significant broadening by approximately 0.3 eV relative to the F 1s emission from crystalline MgF$_2$ (Table 2). However, we also found that an asymmetry on the high-BE side of the emissions could be fitted with a weak additional peak at BEs above 687 eV, which was again particularly strong in MgF$_2$-71. This high-BE peak supports the suggestion that F species with a significant deficiency in electron density are present in the high-surface-area MgF$_2$ samples, suggesting that the local chemical composition in the vicinity of some species leads to a reduction of electron density. These findings support the results of the ^{19}F NMR analysis, which also suggested the presence of a significant amount of F species with electronic structure significantly different from that in crystalline MgF$_2$ of an exact 1:2 molar composition.

The implied deviation from the ideal chemical composition in the surface region of the samples was further supported by analysis of the emissions related to oxygen (Figure 11). First, we detected weak but significant bulk-sensitive O 2s emissions from all of the non-crystalline samples (Figure 11), whereas no such emissions were detectable for a crystalline MgF$_2$ sample. This suggests that the non-crystalline samples contained a small amount of bulk oxygen species. Second, for all of the samples, the surface region, as probed by the O 1s emission, contained significantly higher concentrations of oxygen species than MgF$_2$-C. Again, this
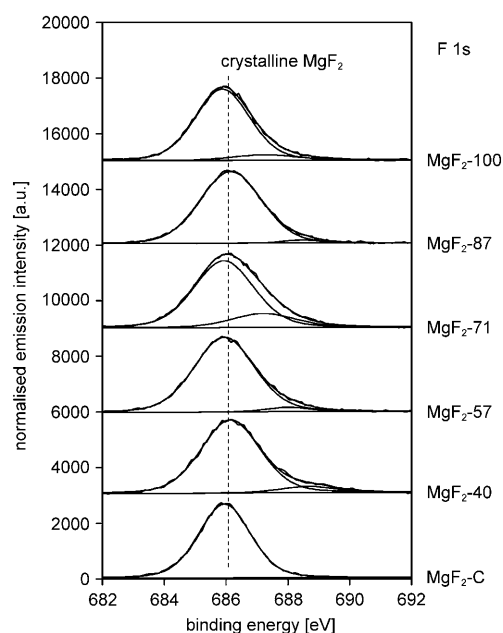

Figure 10. F 1s emissions from the various samples. All spectra have been scaled to approximately the same intensity at the maximum of the emission line.
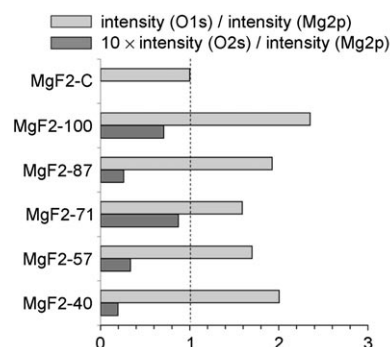

Figure 11. Bulk vs surface emission intensities for oxygen. Light-grey bars: ratios of the intensities of the emissions from O 1s and Mg 2p; dark-grey bars: ratios of the intensities of the emissions from O 2s and Mg 2p.

strongly supports the suggestion derived from analysis of the XPS emission from fluorine that non-stoichiometry at the surface is more significant than in the bulk.

To identify the nature of the oxygen species, we examined the O 1s emissions of Mg(OH)$_2$ and MgO, which were found at 531.2 and 529.6 eV (Table 2), respectively, in good agreement with previous work.[32,33] Note that MgO contains a significant concentration of Mg(OH)$_2$ due to partial hydrolysis at the surface (Table 2).

The weak O 1s emission detected in our investigation of crystalline MgF$_2$ was found at a BE of 532.1 eV (Figure 12), which is shifted to higher BE relative to Mg(OH)$_2$ by the appropriate amount to be compatible with adsorbed water.[34]

Elemental analysis and DSC studies indicated that most of the H_2O adsorbed on the samples should be lost under the vacuum conditions of XPS. In line with this, all O 1s emissions of the non-crystalline samples required fitting with two peaks (Figure 12), one of which was centred in the BE region of adsorbed water. Another possibility, but less likely one (see below), is the presence of hydroxidic groups in an environment similar to that in $Mg(OH)_2$. The other peak was centred at a rather high BE of 534.0 ± 0.4 eV, which is indicative of oxygen species that are deficient in electron density relative to hydroxide. We first examined the possibility that carbonate species formed by exposure to air could be the origin of this feature, but we did not detect any evidence for carbonate formation in the C 1s emission, which would also be expected to be strongly BE shifted, appearing at around 289 eV. This leaves only the possibility that the observed electron deficiency at oxygen stems from the formation of $MgF_{2-x}(OH)_x$ species, in which the geminal fluoride ligands strongly withdraw electron density from the hydroxide groups. This electron-withdrawal through the inductive effect of fluoride ligands provides an explanation for the observed strong Brønsted acidity of these materials. It is also instructive to note that in the region of O 1s BEs beyond 534.8 eV, in which crystalline MgF_2 exhibits no O 1s emission intensity at all, all of the non-crystalline samples exhibit significant intensity. The oxygen species responsible for emissions in this region of the spectrum must be extremely electron deficient, and may, for example, be "dangling" OH species formed by coordination to strong Lewis acid sites at which Mg is coordinated by fluoride ligands. Because of the inductive effect of these fluoride ligands, such OH species would be expected to be particularly Brønsted acidic. The intensity in this region of the spectrum decreases in the order MgF_2-71 $\gg$ MgF_2-40, 57 > MgF_2-87,

100. This order of the samples is approximately in line with their observed catalytic activities in the synthesis of tocopherol, and with the observation that MgF_2-71 exhibited by far the strongest evidence for a deviation from ideal chemical composition through its F 1s and Mg 2p emission features.

BET measurements: N_2 and Ar isotherms of MgF_2-71, as a representative of the series of MgF_2 samples, are given in Figure 13. There was almost no capillary condensation, and no hysteresis loop was observed in the N_2 measurement. The adsorption isotherm corresponds to type I character as regards microporosity.[35] Therefore, we analysed the porous structure of the samples with Ar because it is better able to access micropores than the N_2 molecule (Table 3). The Ar isotherms of MgF_2-71 are also shown in Figure 13, which are similar to the N_2 isotherms. Also, the differences in the BET surface areas are not as high compared with those of typical microporous samples. Therefore, these samples may be classified as being on the border between the microporous and mesoporous ranges.
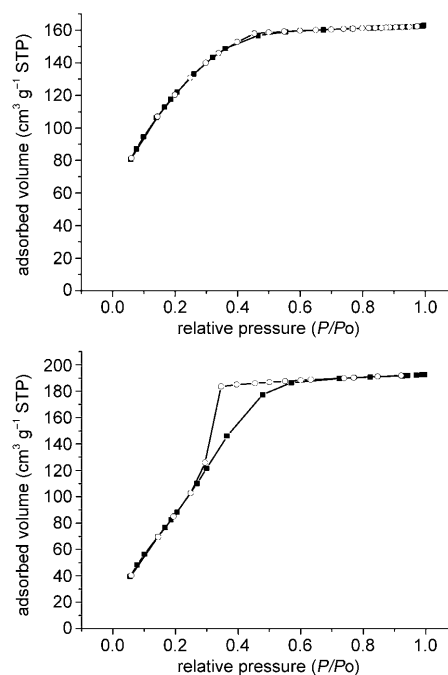
Figure 13. N_2 (top) and Ar (bottom) adsorption isotherms at 77 K of MgF_2-71; ■: adsorption; ○: desorption.

Catalytic tests

As a reaction to test the characteristics of the new magnesium fluoride catalysts, we chose the synthesis of (all-*rac*)-[α]-tocopherol. (all-*rac*)-[α]-Tocopherol displays significant antioxidant properties and has shown promising results in the prevention and treatment of heart disease, cancer, and Alzheimer's disease.[36] As the world population increases from year to year, the production of this compound also increases
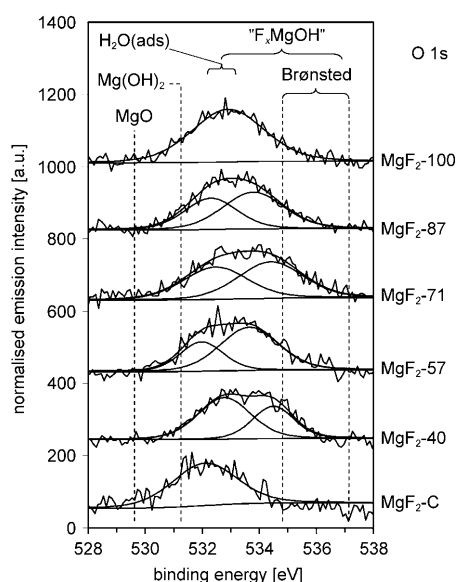
Figure 12. O 1s emissions from the various samples. All spectra have been scaled to approximately the same intensity at the maximum of the emission line.

Table 3. Surface–area properties of the different MgF$_2$ samples measured with N$_2$ and Ar at 77 K (SA = BET surface area; PV = total pore volume; PS = average pore size).

| | MgF$_2$-100 | | MgF$_2$-87 | | MgF$_2$-71 | | MgF$_2$-57 | | MgF$_2$-40 | |
	N$_2$	Ar	N$_2$	Ar	N$_2$	Ar	N$_2$	Ar	N$_2$	Ar
SA [m^2 g^{-1}]	372	441	424	449	264	288	233	253	180	186
PV [cm^3 g^{-1}]	0.21	0.22	0.25	0.25	0.15	0.16	0.14	0.17	0.1	0.12
PS [Å]	20	19	23	22	23	22	24	27	23	26

every year.[37] Besides the practical importance, this synthesis is also interesting as a suitable test reaction for the acidic properties of a catalytic material. The synthesis consists of two steps: 1) Friedel–Crafts alkylation of trimethylhydroquinone (TMHQ, **1**) with isophytol (IP, **2**) to form a phytilhydroquinone intermediate (PHQ, **3**), and 2) chromane ring-closure with the formation of the tocopherol (**4**) (Scheme 2).

It is generally accepted that Friedel–Crafts reactions require Lewis acids when using alkyl halides, but Brønsted acids when the alkylation reagent is an alcohol.[38] Therefore, it can be assumed that the first synthetic step should take place mainly at Brønsted acid sites on the surfaces of the catalyst samples.
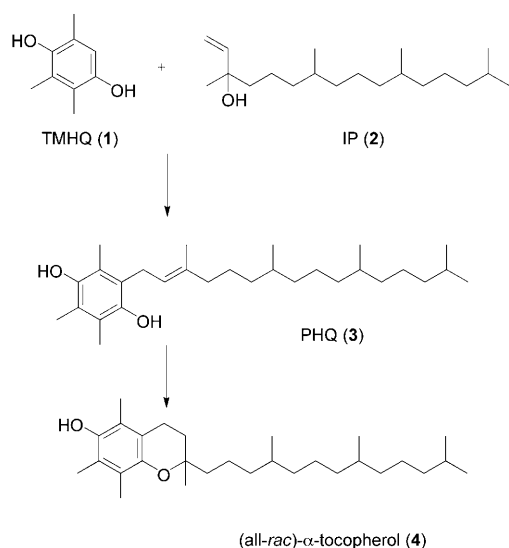
Scheme 2. Synthesis of (all-*rac*)-[α]-tocopherol (**4**) through the condensation of 2,3,5-trimethylhydroquinone (TMHQ, **1**) with isophytol (IP, **2**).

When nanoscopic magnesium fluorides were employed as heterogeneous catalysts in the synthesis of tocopherol, complete conversion of IP was accomplished in less than 1 h and the desired product was obtained with selectivities in the range of 76.3–87.0% depending on the nature of the catalyst. Noteworthy results are shown in Table 4. In comparison, commercial crystalline MgF$_2$ (MgF$_2$-C, Table 4, entry 1) proved to be inactive in this synthesis of

(all-*rac*)-[α]-tocopherol, which was expected because of its almost chemically inert surface having only very weak acid-base centres.

Although the MgF$_2$-40 and MgF$_2$-57 samples, with preponderently Brønsted acid character, showed excellent catalytic activity, (all-*rac*)-[α]-tocopherol was obtained in less than 83% yield. On the other hand, MgF$_2$-87 and MgF$_2$-100 were not effective under the same conditions, with the IP remaining completely unconverted even after 5 h. Thus, the Lewis acid sites (MgF$_2$-87 and MgF$_2$-100) of moderate strength do not seem to be sufficient to promote the synthesis of (all-*rac*)-[α]-tocopherol, and IR experiments have shown that these compounds do not have Brønsted sites. The best yields of (all-*rac*)-[α]-tocopherol were obtained in the presence of the MgF$_2$-71 sample (Table 4, entry 4). At the moment, it is not entirely clear as to whether the total number of acidic sites has an influence upon the synthesis, but it is obvious that the presence of Brønsted acid sites is essential to promote the first synthetic step, while for the general synthesis the Lewis/Brønsted acid site ratio is a critical feature. It seems that the optimal combination of Lewis/Brønsted acid sites was generated in the sample MgF$_2$-71.

Alcohols, especially tertiary allylic alcohols such as IP, easily lose water in the presence of acids to form highly reactive carbocations. Therefore, the formation of considerable amounts of dehydration products, so-called phytadienes, is a general problem in such procedures. A practical way to avoid this by-product is to use the generally adopted procedure, in which the IP is added dropwise to a stirred mixture of the catalyst and TMHQ dissolved in a suitable solvent.[39] However, we only found small amounts of phytadienes (generally <5%) when TMHQ was reacted with IP, even if the latter was added from the beginning of the process in one single charge. This behaviour was probably due to the medium-strength acidity of our catalysts, as a result of which there was a low capacity for stabilisation of the carbocation, which resulted in less phytadienes. Surprisingly, however,

Table 4. Influence of the key surface features and the reaction parameters on the catalytic performance.

Entry	Catalyst	Number of acid centers/m^2	IP/cat. molar ratio	t [min]	Yield tocopherol [%]
1	MgF$_2$-C	n.d.	n.d.	1800	0
2	MgF$_2$-40	5.4×10^{17}	119	300	76.3
3	MgF$_2$-57	6.6×10^{17}	76	300	82.6
4	MgF$_2$-71	3.6×10^{17}	123	300	87.0
7	MgF$_2$-87	4.8×10^{17}	60	360	0
8	MgF$_2$-100	8.4×10^{17}	37	360	0

Reaction conditions: 50 mg of catalyst; T = 100°C; THQ/IP = 1:1; solvent: heptane/propylene carbonate 50:50. Conversion is based on IP (C = 100%).

the synthesis took place with complete regioselectivity, as long as no benzofuran derivatives were detected in the reaction products. Generally speaking, the regioselectivity of a catalytic reaction depends on the structure of the molecule, the structure of the catalyst, and the reaction conditions, with these factors being highly interdependent. In other words, a comprehensive interpretation of regioselectivity requires that the substrate–catalyst couple be considered as a supramolecular system. Particularly in the condensation of TMHQ with IP, the availability and proportion of the different carbocations, for example, isophytil and *n*-phytil, formed by the interaction of IP with the catalyst, seems to be the key feature for obtaining high regioselectivity in favour of the desired (all-*rac*)-[α]-tocopherol. No quinone compounds were detected, even when reactions were conducted in vessels open to the atmosphere.

Conclusion

The fluorolytic reaction of magnesium methoxide with anhydrous HF in methanolic solution results in the formation of nanoscopic MgF_2, which possesses Lewis acid sites of medium strength. If this synthesis is performed under otherwise identical conditions, but using aqueous HF instead of anhydrous HF, then partly hydroxylated MgF_2 phases are obtained. As a result of competitive hydrolysis, the content of hydroxyl groups in the MgF_2 samples increases with increasing H_2O content in the HF solution. Astonishingly, these hydroxyl groups are not basic in nature, as might be expected for MgOH units, but Brønsted acidic. By varying the HF concentration, $MgF_{2-x}(OH)_x$ phases can be obtained, for which a fine tuning of the ratio of Lewis acidic to Brønsted acidic surface sites becomes possible. However, it has been found that these OH groups are only Brønsted acidic provided that the amount of hydroxyl groups is suitably small ($x < 0.1$). Larger values of x result in the formation of basic OH groups, as expected. We have obtained strong evidence for the formation of $MgF_{6-n}(OH)_n$ octahedral units. Thus, the Brønsted acidity could be due to hydrogen bonding between the H of OH and neighbouring F atoms. Obviously, if the OH content is too high, neighbouring OH groups will more likely be encountered, and this will induce basic sites instead of acidic ones. If the synthesis is performed in such a way that a substoichiometric amount of HF is added first, followed by the requisite amount of H_2O, then the phases obtained do not behave as Brønsted acids.[6] At this point, we can only speculate, albeit with the support of TEM, MAS NMR, and XPS results, that the synthesis using stoichiometric HF (HF:Mg=2) but containing some water results in shell-like nanoparticles of $MgF_{2-x}(OH)_x$ phases, the inner cores (bulk) of which mainly consist of essentially pure MgF_2. In their outer shells (surface), they become increasingly hydroxylated (with x still < 0.1), as evidenced by XPS and FTIR results. This is because the competing hydrolysis reaction becomes increasingly relevant after the fluorolysis reaction has consumed the HF in the re-action system. However, we are confident that there are no regions in the nano-$MgF_{2-x}(OH)_x$ particles in which the OH content becomes dominant over the F concentration. Thus, a very promising new class of solid Lewis–Brønsted acidic catalysts can be obtained in this way, which show both high activity and selectivity in the synthesis of (all-*rac*)-[α]-tocopherol.

Acknowledgements

[1] S. Rüdiger, U. Groß, E. Kemnitz, *J. Fluorine Chem.* **2007**, *128*, 353.
[2] S. Rüdiger, E. Kemnitz, *Dalton Trans.* **2008**, 1117.
[3] J. K. Murthy, U. Groß, S. Rüdiger, E. Kemnitz, *J. Solid State Chem.* **2006**, *179*, 739.
[4] S. Wuttke, G. Scholz, S. Rüdiger, E. Kemnitz, *J. Mater. Chem.* **2007**, *17*, 4980.
[5] M. N. Amiry, G. Eltanany, S. Wuttke, S. Rüdiger, E. Kemnitz, J. M. Winfield, *J. Fluorine Chem.* **2008**, *129*, 366.
[6] H. A. Prescott, Z.-J. Li, E. Kemnitz, J. Deutsch, H. Lieske, *J. Mater. Chem.* **2005**, *15*, 4616.
[7] M. Wojciechowska, M. Zielinski, M. Pietrowski, *J. Fluorine Chem.* **2003**, *120*, 1.
[8] M. Wojciechowska, B. Czajka, M. Pietrowski, M. Zielinski, *Catal. Lett.* **2000**, *66*, 147.
[9] H. Kabashima, H. Tsuji, H. Hattori, *Appl. Catal. A* **1997**, *165*, 319.
[10] T. Seki, H. Kabashima, K. Akutsu, H. Tachikawa, H. Hattori, *J. Catal.* **2001**, *204*, 393.
[11] M. A. Aramendia, V. Borau, C. Jimenez, J. M. Marinas, J. R. Ruiz, F. J. Urbano, *Appl. Catal. A* **2003**, *244*, 207.
[12] D. G. Cory, W. M. Ritchey, *J. Magn. Reson.* **1988**, *80*, 128.
[13] S. Brunauer, P. H. Emmett, E. Teller, *J. Am. Chem. Soc.* **1938**, *60*, 309.
[14] M. P. Seah, *Surf. Interface Anal.* **2001**, *31*, 721.
[15] C. R. S. Beatrice, W. Garlipp, M. Cilense, A. T. Adorno, *Scripta Metallurgica et Materialia* **1995**, *32*, 23.
[16] V. Karpus, A. Suchodolskis, U. O. Karlsson, L. Giovanelli, W. Assmus, S. Bruhne, E. Uhrig, *Appl. Surf. Sci.* **2006**, *252*, 5411.
[17] Y. Diao, W. Walawender, C. S. Sorensen, K. J. Klabunde, T. Ricker, *Chem. Mater.* **2002**, *14*, 362.
[18] K. T. Ranjit, K. J. Klabunde, *Chem. Mater.* **2005**, *17*, 65.
[19] *EP Pat.* **2007**, 07020498.7.
[20] W. H. Baur, A. A. Khan, *Acta Crystallogr. Sect. B* **1971**, *27*, 2133.
[21] R. König, G. Scholz, E. Kemnitz, *J. Fluorine Chem.* **2008**, *129*, 598.
[22] J. A. Lercher, C. Gründling, G. Eder-Mirth, *Catal. Today* **1996**, *27*, 353.
[23] T. Krahl, A. Vimont, G. Eltanay, M. Daturi, E. Kemnitz, *J. Phys. Chem. C* **2007**, *111*, 18317.
[24] G. Spoto, E. N. Gribov, G. Ricchiardi, A. Damin, D. Scatano, S. Bordiga, C. Lamberti, A. Zecchina, *Prog. Surf. Sci.* **2004**, *76*, 71.
[25] L. Oliviero, A. Vimont, J.-C. Lavalley, F. R. Sarria, M. Gaillard, F. Mauge, *Phys. Chem. Chem. Phys.* **2005**, *7*, 1861.
[26] J.-C. Lavalley, *Catal. Today* **1996**, *27*, 377.
[27] C. Morterra, G. Magnacca, *Catal. Today* **1996**, *27*, 497.
[28] J. Lercher, C. Colombier, H. Noller, *J. Chem. Soc. Faraday Trans. 1* **1984**, 949.
[29] C. Morterra, A. Zecchina, S. Coluccia, A. Chiorino, *J. Chem. Soc. Faraday Trans. 1* **1977**, 1544.
[30] G. Busca, V. Lorenzelli, *Mater. Chem.* **1982**, *7*, 89.

[31] C. J. Powell, A. Jablonski, NIST Electron Effective-Attenuation-Length Database, version 1.0, National Institute of Standards and Technology, Gaithersburg, MD, **2001**.

[32] D. K. Aswal, K. P. Muthe, S. Tawde, S. Chodhury, N. Bagkar, A. Singh, S. K. Gupta, J. V. Yakhmi, *J. Cryst. Growth* **2002**, *236*, 661.

[33] J. H. Lee, J. H. Eun, S. G. Kim, S. Y. Park, M. J. Lee, H. J. Kim, *J. Mater. Res.* **2003**, *18*, 2895.

[34] J. T. Kloprogge, L. V. Duong, B. J. Wood, R. L. Frost, *J. Interf. Coll. Sci.* **2006**, *296*, 572.

[35] A. J. Lecloux, in *Catalysis: Science and Technology, Vol. 2* (Eds.: J. R. Anderson, M. Boudart), Springer, Berlin, **1983**, p. 171.

[36] T. Netscher, *Chimia* **1996**, *50*, 563.

[37] W. Bonrath, M. Eggersdorfer, T. Netscher, *Catal. Today* **2007**, *121*, 45.

[38] A. Corma, H. Garcia, *Chem. Rev.* **2003**, *103*, 4307.

[39] K. Ishihara, M. Kubota, H. Yamamoto, *Synlett* **1996**, 1045.